Article:
Zhang, M, Bi, C, Xia, Y et al. (7 more authors) (2023) Water-Driven Synthesis of Deep-Blue Perovskite Colloidal Quantum Wells for Electroluminescent Devices. Angewandte Chemie, 62 (12). e202300149. ISSN 0044-8249

https://doi.org/10.1002/anie.202300149

RESEARCH ARTICLE

Water-Driven Synthesis of Deep-Blue Perovskite Colloidal Quantum Wells for Electroluminescent Devices

Mengqi Zhang[+], Chenghao Bi[+], Yuexing Xia, Xuejiao Sun, Xingyu Wang, Aqiang Liu, Shuyu Tian, Xinfeng Liu, Nora H. de Leeu, Jianjun Tian*

M. Zhang, Dr. C. Bi, A. Liu, S. Tian, Prof. J. Tian
Institute for Advanced Materials and Technology
University of Science and Technology Beijing
Beijing 100083, China
and
Shunde Innovation School
University of Science and Technology Beijing
Foshan, Guangdong, 528399, China
[*] E-mail: tianjianjun@mater.ustb.edu.cn
Y. Xia, Prof. X. Liu
CAS Key Laboratory of Standardization and Measurement for Nanotechnology
Beijing National Center for Nanoscience and Technology
Beijing, 100190, China
and
University of Chinese Academy of Sciences
Beijing, 100049, China
Dr. X. Sun
Institute of Semiconductors Chinese Academy of Sciences
Beijing, 100083, China.
X. Wang, Prof. N. H. de Leeu
School of Chemistry
University of Leeds
Leeds, LS2 9JT, UK.
[+] These authors contributed equally to this work.

Abstract: Perovskite colloidal quantum wells (QWs) are promising to realize narrow deep-blue emission, but the poor optical performance and stability suppress their practical application. Here, we creatively propose a water-driven synthesis strategy to obtain size-homogenized and strongly confined deep-blue $CsPbBr_3$ QWs, corresponding to three monolayers, which emit at the deep-blue wavelength of 456 nm. The water controls the orientation and distribution of the ligands on the surface of the nanocrystals, thus inducing orientated growth through the Ostwald ripening process by phagocytizing unstable nanocrystals to form well-crystallized QWs. These QWs present remarkable stability and high photoluminescence quantum yield of 94%. Furthermore, we have prepared light-emitting diodes based on the QWs via the all-solution fabrication strategy, achieving an external quantum efficiency of 1% and luminance of 2946 cd m^{-2}, demonstrating state-of-the-art brightness for perovskite QW-based LEDs.

Introduction

Cesium lead halide ($CsPbX_3$; X = Cl, Br, and I) perovskite nanocrystals have recently attracted a great deal of attention for their intriguing properties, including intrinsic defect tolerance, nearly unity photoluminescence quantum yield (PLQY), emission tunability, and facile solution-process fabrication.[1] These unique properties make them the most promising candidates for practical applications in high-definition displays. Recently, red and green light-emitting diodes (LEDs) based on perovskite nanocrystals have shown significant improved efficiency, showing an external quantum efficiency (EQE) of over 20%, [2] which is comparable to those of organic LEDs. However, the EQE of the blue LEDs lags behind that of their red and green counterparts, especially for deep-blue (≤ 460 nm) ones. [3] Therefore, it is important to thoroughly investigate and develop highly efficient and stable perovskite LEDs with the desired blue wavelength.

To date, composition engineering of mixed halides such as $CsPb(Br_xCl_{1-x})_3$ is commonly applied to adjust the blue emission wavelengths of perovskites. Nevertheless, the mixed-halide perovskites are plagued by phase instability issues stemming from extensive ion migration under illumination and voltage bias. [4] Another widely employed strategy to achieve blue emission is referred to as dimensional engineering, which utilizes the quantum confinement effect to tune the band gap to the desired emission wavelength. Significant efforts have been made on the colloidal synthesis of strong-confined perovskite nanocrystals with tunable morphologies, involving nanoparticles, nanorods, nanowires, and nanoplatelets. [2a, 5] Among these, the colloidal quantum wells (QWs), also referred to as nanoplatelets, have shown significant potential for the fabrication of efficient blue LEDs, owing to their tunable optical properties at the molecular level, narrow emission wavelength with suppressed inhomogeneous broadening, and notable optical non-linearities. [6] However, the long-chain organic

ligands limit the charge transfer, whereas ligands with reduced chain-lengths induce uncontrolled thickness distribution of the perovskite QWs. [7] Recently, perovskite QWs obtained by Wang *et al.*, who used short-chain ligands such as ammonium bromide (NH_4Br) and butylamine (C4) to improve the charge mobility of the perovskite QWs films when constructing LEDs. [8] However, the overall PLQYs were observed to be in the range of 64% to 71%, indicating that there was still potential to further improve the optical performance of the perovskite QWs. Additionally, solution-processed QWs generally contain a distribution of several well-widths, which may contribute to non-radiative recombination loss and broadened emissions.[9] Considering these two main opportunities to prepare improved LEDs, here we propose a water-driven synthesis strategy to obtain perovskite QWs with improved crystallinity and size homogeneity. The water is able to control the orientation of the ligand distribution on the surface of the QWs. Those QWs with defective crystal facets have high surface energies, thus inducing the orientation growth towards the (100) plane by phagocytizing unstable nanocrystals based on the Ostwald ripening process. As a result, the homogenous QWs present narrow full width at half maximum (FWHM) of 20 nm with a single PL emission peak at 456 nm, corresponding to three monolayers (MLs). More importantly, the QWs present high PLQY of 94 %, which is attributed to high crystal quality and reduced surface defects. Furthermore, the LEDs based on the QWs show an EQE of 1% and luminance of 2946 cd m^{-2}, which is the highest luminance value reported so far for blue perovskite LEDs based on QWs.

Results and Discussion

We have developed a novel strategy to synthesize $CsPbBr_3$ QWs based on the conventional hot-injection method (Figure 1a). Briefly, the pristine $CsPbBr_3$ QWs are first prepared by swiftly injecting Cs-Oleate into the $PbBr_2$ precursor at 105 °C, followed by ice-water cooling to 40 °C. The water-driven synthesized (WD-synthesized) QWs are obtained by injecting purified water into the pristine sample reheated at 70 °C, stirring for ~ 30 s (see the Experimental section for further details).

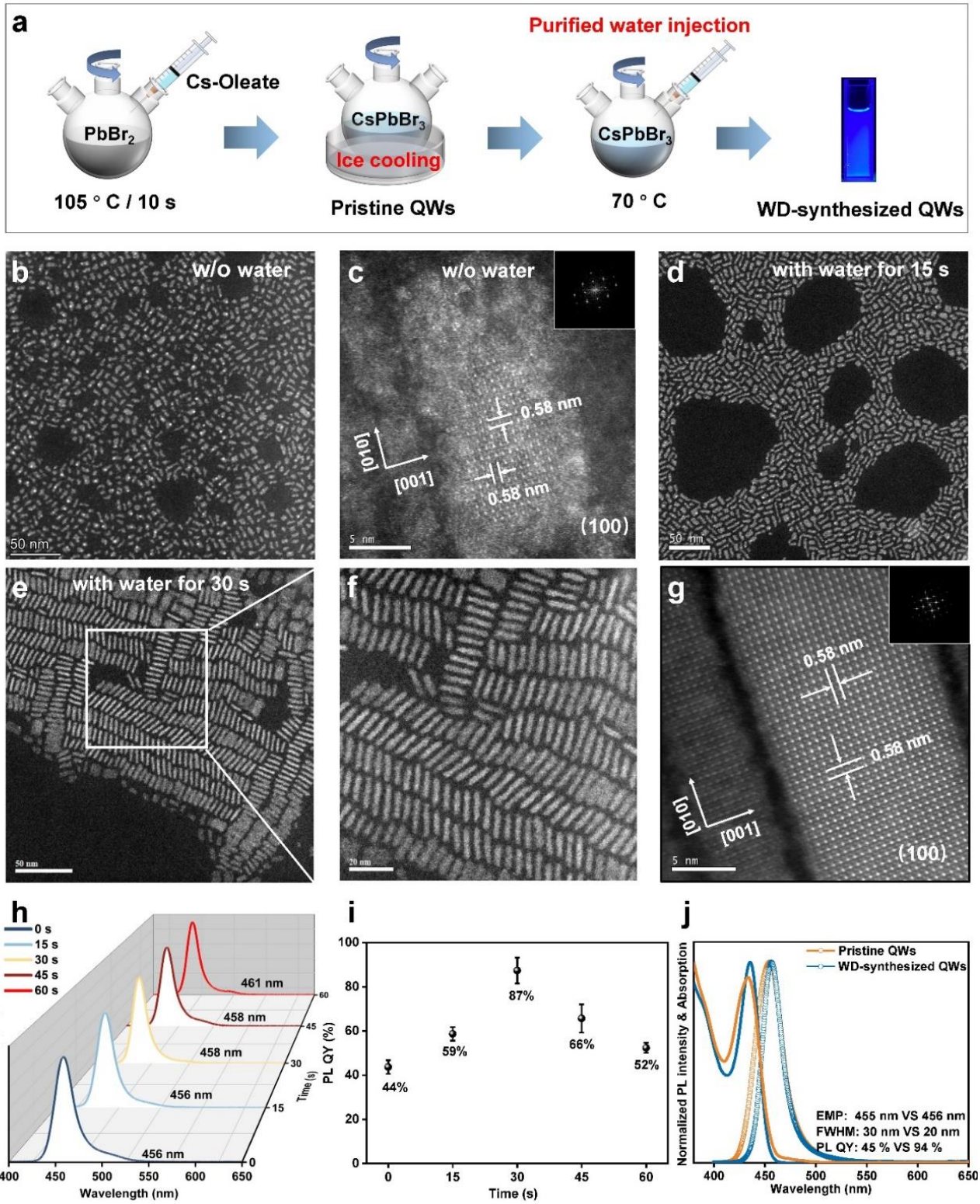

Figure 1. Fabrication, morphology and optical performance of the QWs. (a) Illustration of the water-driven synthesis process of QWs. (b-c) TEM and HRTEM images of the QWs without water addition. (d) TEM image of the QWs with water addition for 15 s. (e-g) TEM and HRTEM images of the QWs with water addition for 30 s. (h) PL profile. (i) PLQY of the QWs with added water at different stages (0 s, 15 s, 30 s, 45 s, and 60 s). (j) PL and absorption spectra of the pristine QWs and QWs with 40 μL water addition for 30 s.

Figures 1b-g show the transmission electron microscopy (TEM) and high-resolution TEM (HRTEM) images of the perovskite QWs at different reaction stages, including the pristine product without the introduction of water and the QWs with water introduced for 15 s and 30 s, respectively. Initially, the obtained QWs without water addition present poor crystal quality, low crystallite coverage rate, and irregular shape distribution (Figure S1a). After introducing water for 15 s, the ultra-small QWs and nanocrystals disappear, while the uniform-sized QWs are obtained (Figure S1b), indicating that the addition of water might prompt the oriented crystallization of the QWs. When the reaction period is further extended, all QWs show high crystallinity with vertical stacking in a face-to-face manner (Figure S2). The size distribution of the final QWs satisfies the Gaussian distribution much better than the initial stage (Figure S3). The average thickness of 2.3 ± 0.02 nm (length of 12.5 ± 0.17 nm) corresponds to three MLs of the unit cell in perovskites, which is in accordance with the deep-blue spectrum achieved by the strong quantum confinement.[8] The crystal structure is illustrated in Figure S4, indicating that the quantum confinement effect is dominant along the thickness direction of QWs. Compared with the HRTEM images of the QWs without/with addition of water (Figures 1c and g), there is no significant change in the d-spacing, which remains 0.58 nm, corresponding to the (100) crystal plane of the cubic $CsPbBr_3$ phase, which illustrates that the intrinsic crystal structure is unaffected by water. Meanwhile, various crystal facets of the pristine sample (without addition of water) are exposed because of poor crystallinity, resulting in atomic vacancies in the surface. The WD-synthesized QWs possess regular rectangle shape with the perfect crystal structure, and defects are rarely detected in the field of view, while the lattice extends along the [010] direction. Note that a set of diffraction peaks with a period of 6.7 º is observed at small angles in the X-ray diffraction (XRD) results (Figure S5), corresponding to the pristine QWs with a thickness of 1.3 nm. The periodic diffraction pattern disappears in the WD-synthesized QWs, indicating that those QWs with ultra-small size are eliminated by water introduction, and the overall crystal quality is improved. Moreover, the elemental mapping images (Figure S6) indicate that the distribution of elements in the WD-synthesized QWs remains uniform, revealing that only the morphology is affected by the incorporation of water.

Such structural evolution is associated with change in the optical performance of the QWs. Figure 1h shows the PL spectra of the objects at different stages after injection of water, and the corresponding absorption profile is given in Figure S7. It can be seen that the PL and absorption spectra of the QWs present a minor redshift as the reaction duration is extended. An additional emission peak at ~520 nm shows up when the reaction time reaches 60 s, which is attributed to the further growth of the QWs along the thickness direction (quantum confinement effect direction) because of the dynamic desorption of surface ligands of the QWs (oleic acid (OA), oleylamine (OAm)),[10]

indicating a suitable reaction period is essential. Taking PLQY as a criterion (Figure 1i), the maximum value of 94% (the average value is 87%) is obtained when the reaction duration is 30s, suggesting high crystal quality and low trap density for the products at this stage. The effect of adding water on the optical performance of the QWs is also studied (Figures S8-10). The results demonstrate that the appropriate amount of water to be added is 40 μL. An additional PL emission peak position at ~ 515 nm is observed when the added amount is more than 70 μL, which might stem from some oversized QWs under water-rich condition.[11] More detailed results are summarized in Figure S11 and Tables S1-2. Compared to the pristine sample, the final WD-synthesized QWs possess a similar emission peak but a sharper exciton peak (Figure 1j), illustrating that the quantum confinement effect is maintained while improving their crystallinity. The narrower FWHM (30 nm to 20 nm) and improved PLQY (45% to 94%) of the WD-synthesized QWs arise from the better crystallization and size distribution, and their surface might subsequently be passivated or modified by water-driven surface reconstruction.[12] A PL spectrum *in situ* tracking system is set up to reveal the formation mechanism of the QWs with the addition of water (Figure 2a). Figures 2 b-c represent the spectral evolution of two samples during the synthesis process. The PL intensity of the pristine QWs slightly decreases with time, owing to desorption of surface ligands and high-temperature fluorescence quenching, [13] while that of the WD-synthesized QWs increases after the introduction of water, indicating reduction of the defect density. In addition, the emission intensity enhanced region of the WD-synthesized QWs is much narrower than that of the pristine QWs, which is confirmed by the instant FWHM recording (Figure 2d). Figure 2e shows the terminal emission distribution of two samples. The pristine sample exhibits blue emission with two prominent PL emission peaks at around 441 nm and 456 nm, corresponding to 2 MLs and 3 MLs nanoplatelets, respectively. [11b] An obvious band tail is also fitted at 468 nm, which might result from the generation of significant defects, whereby excitons recombine through a non-radiative process.[14] The PL profile of the WD-synthesized QWs is more symmetrical with a single emission peak at 455 nm and suppressed band tail, suggestive of the improved crystal quality and size distribution.

Knowing that the surface ligands control the growth orientation of nanocrystals, [15] calculations based on the density functional theory (DFT) are employed to assist in elucidating the interactions between the ligands and crystal facets. The DFT results (Figure 2f) provide adsorption energies (E_{ads}) of the [OA, OAm], adsorbed on the (100), (110) and (111) crystal planes of [-0.45, -0.38 eV], [-0.18, -0.17 eV], and [-0.41, -0.36 eV], respectively. The strongest interactions of OA and OAm could stabilize the (100) and (111) planes, because the attached ligands would retain surface ions and act as ionic anchoring sites. [5g] In contrast, vacancies are more likely to be generated on the (110) crystal planes as the adsorption energy is weaker. As such, the strong surface-ligand interactions would favor

the formation of more regular nanocrystals with fewer defects.

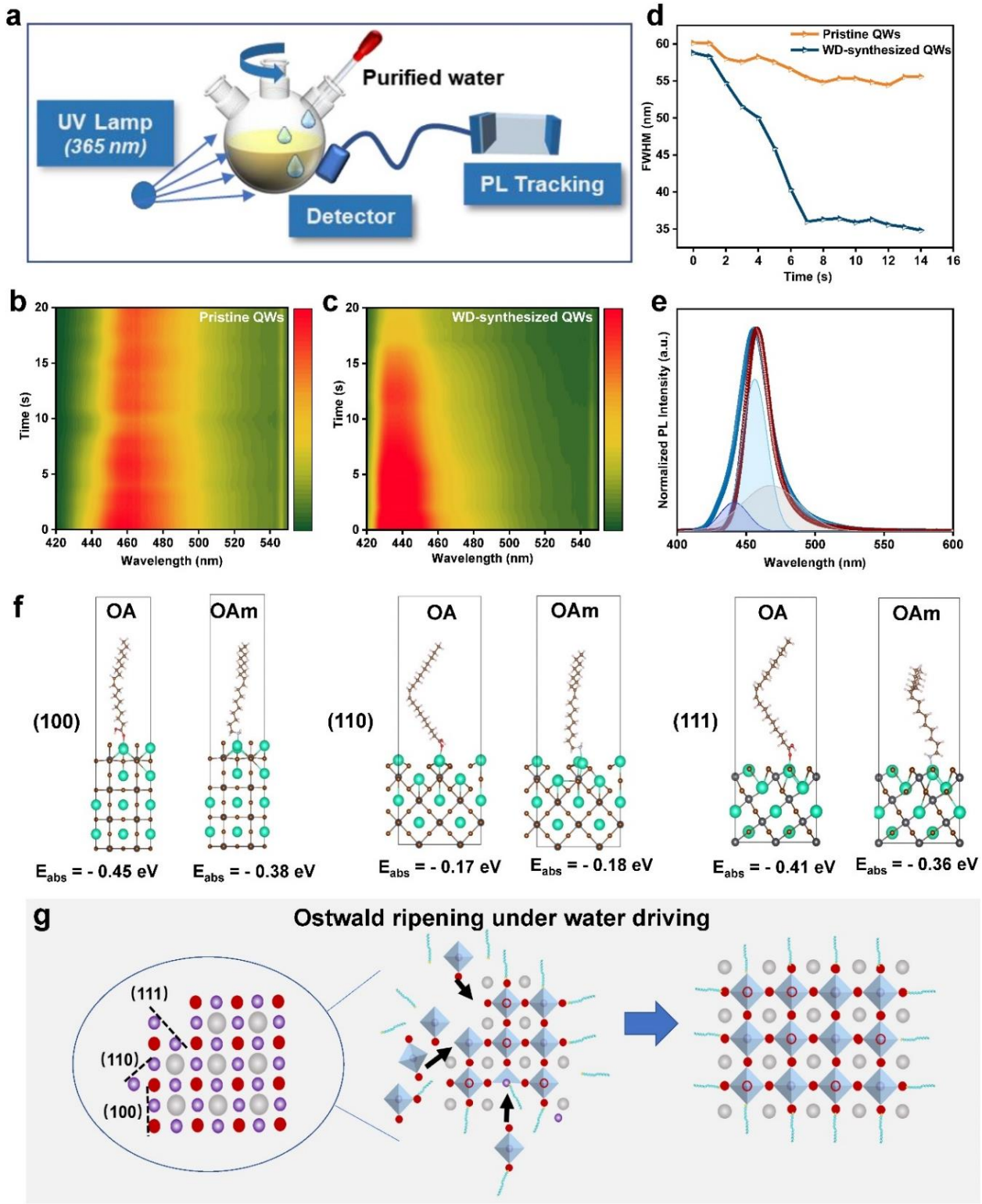

Figure 2. Formation process of the WD-synthesized QWs. (a) Illustration of the in-situ PL spectra monitoring system. Color map of spectral evolution of (b) the pristine and (c) the WD-synthesized QWs, respectively. (d) FWHM and (e) PL intensity variance of the pristine and WD-synthesized QWs. (f) DFT calculations of the adsorption energies of ligands (OA and OAm) at the QW surfaces. (g) Illustration of the mechanism of the evolution of the morphology of the WD-synthesized QWs.

Based on the results above, the mechanism of the WD-synthesized QWs can be illustrated in Figure 2g. There are many more defects in the surfaces of the pristine QWs because of their intrinsically unstable nature. In addition, the surfaces of the pristine QWs are randomly and dynamically capped with ligands, which are labile and sensitive to polar solvents (such as water). [10] Knowing that the binding energy between the ligands and the (100) crystal facet is the strongest, after introducing water into the crude solution, highly dynamic ligands could be dissociated from the other facets, exposing the pristine QWs with defective layers at the surface. Those defective crystal facets are highly reactive, which induces reconstruction of the QWs involving neighboring particles until all exposed facets are (100) plane, where the strongly bound ligands passivate the surfaces. [5a, 16] Meanwhile, some unstable QWs of ultra-small size are phagocytized by the bigger QWs to form high-quality QWs with a homogenized phase distribution based on the Ostwald ripening theory. [17] Those fully evolved WD-synthesized QWs finally show better crystallinity and a uniform size distribution, which is consistent with their high optical performance.

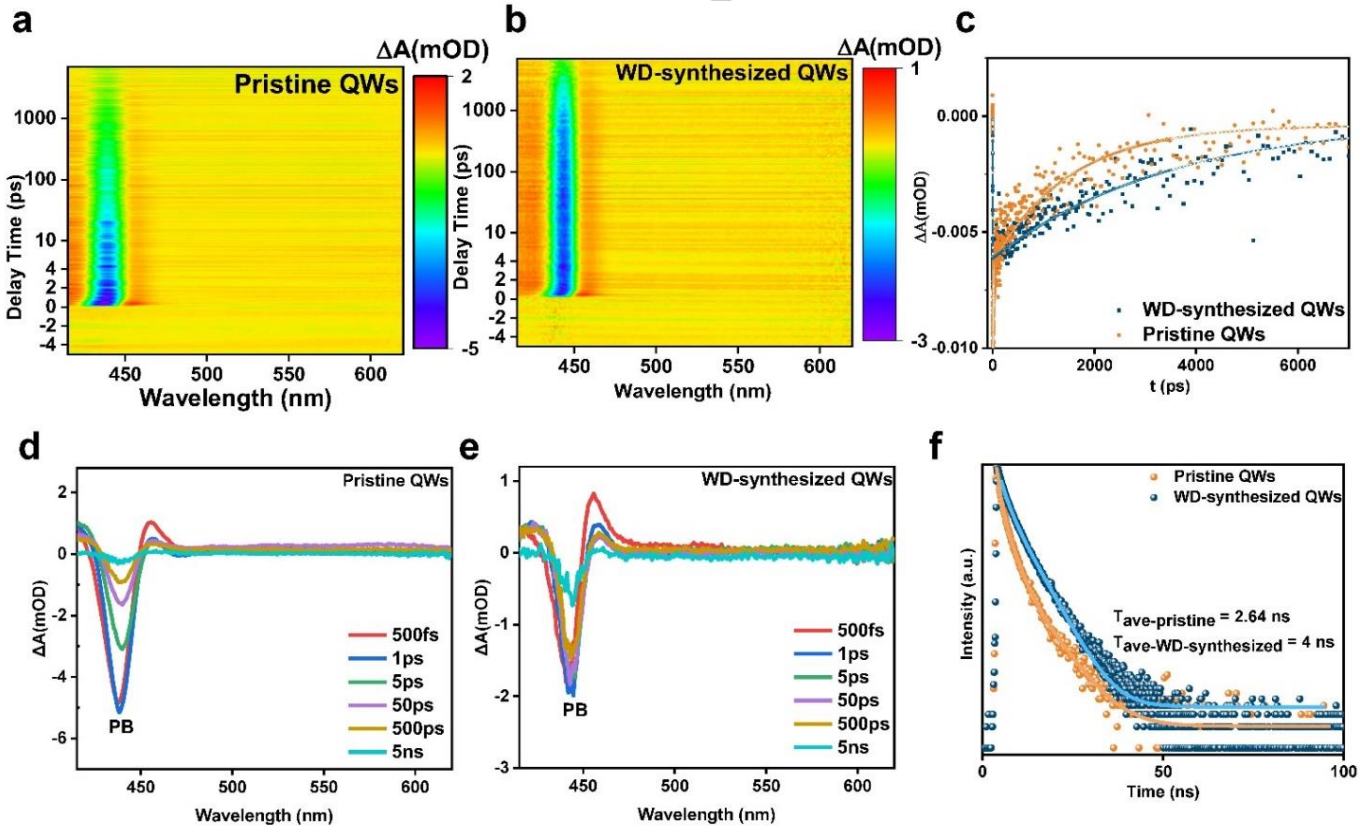

Figure 3. Exciton dynamics of the QWs. The 2D pseudo-color fs-TA plots of (a) the pristine and (b) the WD-synthesized QWs. (c) TA comparisons of bleach recovery dynamics of the pristine and WD-synthesized QWs. The fs-TA spectra of (d) the pristine and (e) the WD-synthesized QWs at different delay times. (f) TRPL decay of the pristine and WD-synthesized QWs.

Ultrafast femtosecond transient absorption (TA) is conducted to gain further insight into the

mechanism behind the intriguing photo-physical properties of the QWs. As shown in the 2D pseudo-color TA plots (Figures 3 a-b), the WD-synthesized QWs show enhanced and narrower ground-state bleaching (GSB) in comparison with the pristine QWs, which is attributed to the decrease of trap density for the WD-synthesized QWs. [18] In addition, the spectral diffusion of the WD-synthesized QWs is suppressed with time, indicating the trap density is reduced near the band-edge, [18,19] which is confirmed by the higher PLQY of the WD-synthesized QWs. The optical absorption change (ΔA) is depicted in Figures 3 d-e, which exhibits a negative bleaching signal (PB) with two small positive signals on bilateral sides. Both samples give obvious PB signals at 437 nm and 439 nm, matching the energy of the first exciton transition in the linear absorption of 435 nm and 436 nm, respectively. The spectrum shape of the pristine QWs remains almost unchanged for 5 ps with negligible redshift; the time to maintain the stable spectral line becomes longer for the WD-synthesized QWs (almost 250 ps). As it is known that the bi-exciton recombination dominates the decay process, [5b, 20] the increased decay time of the WD-synthesized QWs reveals a stronger exciton-exciton interaction. In combination with the bleach recovery dynamics (Figure 3c and Table S3), the pristine sample exhibits bi-exponential bleach recovery dynamics with an ultrafast component of 10.6 ps (τ_1) and a longer component of 1508 ps (τ_2). However, the WD-synthesized QWs present single-exponential decay dynamics with one time constant of 3437.8 ps, revealing that the non-radiative recombination paths are effectively suppressed, and excited carriers are efficiently utilized. [21] This consequence is consistent with the results of the time-resolved PL measurements (TRPL). As shown in Figure 3f (and Tables S4-5), the WD-synthesized QWs exhibit a bi-exponential PL decay with an average lifetime of 4.0 ns, i.e., longer than that of the pristine sample (2.6 ns), indicating that non-radiative recombination in the WD-synthesized QWs is eliminated through efficient surface defect reduction, which can be verified further by the radiative rate. The WD-synthesized QWs have a faster radiative rate (0.24 ns^{-1}) and suppressed non-radiative rate (0.01 ns^{-1}), compared with the pristine counterpart (0.17 ns^{-1} and 0.21 ns^{-1}, correspondingly). In summary, the carrier dynamics of the WD-synthesized QWs are slower than that of their pristine counterparts, indicating that the band gap might be renormalized in QWs, showing stronger Coulombic interactions and higher exciton binding energies, [21a] which is verified by the temperature-dependent PL measurements (100 – 300 K), shown in Figure S12. The fitting results give E_b values of 288.69 eV and 471.17 eV for the pristine and WD-synthesized QWs, respectively. The increased E_b is theoretically beneficial in QWs to keep excitons dynamic and allow more efficient recombination. [22]

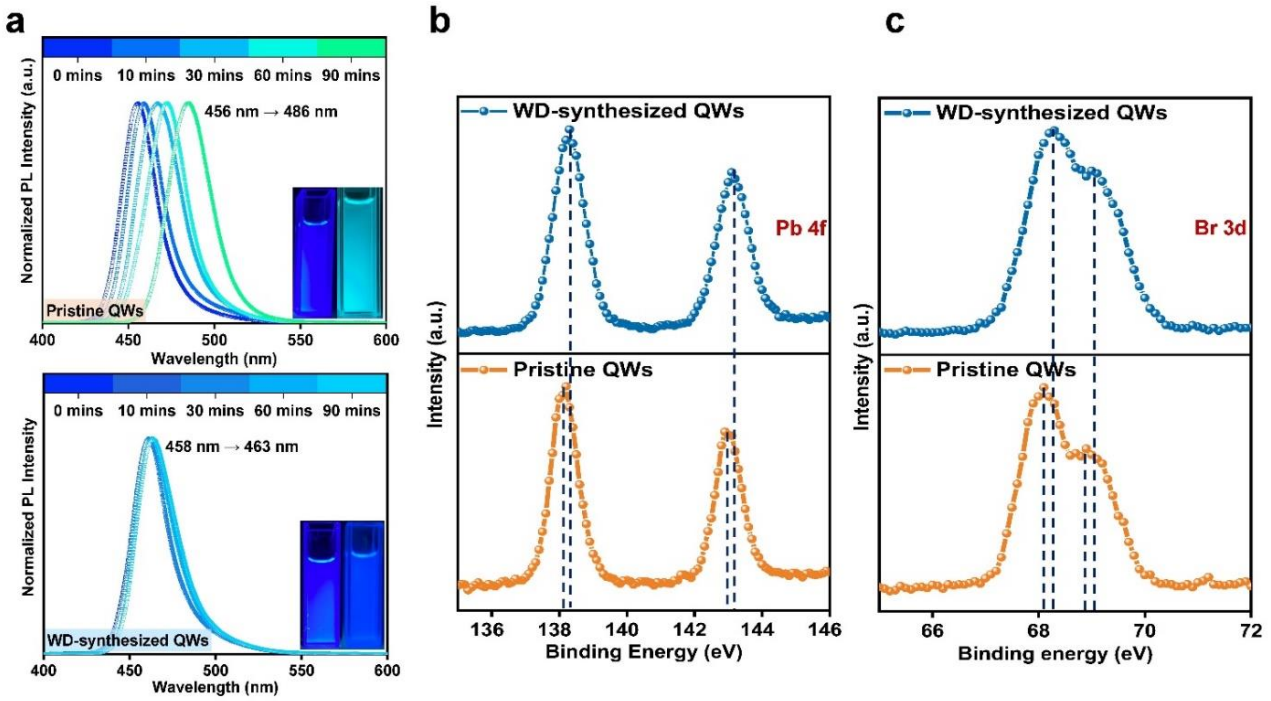

Figure 4. Spectral stability of the QWs. (a) PL intensity profiles of the pristine and WD-synthesized QWs after UV-light irradiation for various periods, as indicated in the frame. XPS spectra of (b) Pb-4f and (c) Br-3d of the pristine and the WD-synthesized QWs, respectively.

Considering that the ligands are actively dynamic under ultraviolet (UV) immersion, thereby inducing spectral instability and degradation of optical performance, [23] we assess the spectral stability of the QWs by monitoring the solution under continuous UV-light irradiation (365 nm wavelength). With increasing irradiation time, the PL peak position of the pristine sample shows a progressive redshift (from 456 nm to 486 nm) and a distinct change in their emission color (Figure 4a). In contrast, the WD-synthesized QWs preserve the emission position and intensity under the same condition, revealing excellent long-term stability. By quantifying the profile of the Fourier-transformed infrared spectroscopy (FITR), shown in Figure S13, we observe no noticeable vibration signal difference between the two samples, suggesting that the surface ligands are unaffected by water. Additionally, X-ray photoelectron spectroscopy (XPS) analysis is performed to verify the surface coordination environment of the QWs. Compared to the pristine sample, the WD-synthesized QWs show gradual shifts to higher binding energies for Pb 4f and Br 3d (Figures 4 b-c, respectively), implying stronger Pb-Br interaction in the $[PbBr_6]^{4-}$ octahedra. Therefore, the suppressed coalescence in the solution under relatively intense UV radiation is attributed to the stronger binding energy for the WD-synthesized QWs, which benefit from their high crystallinity and low defect density, as discussed previously.

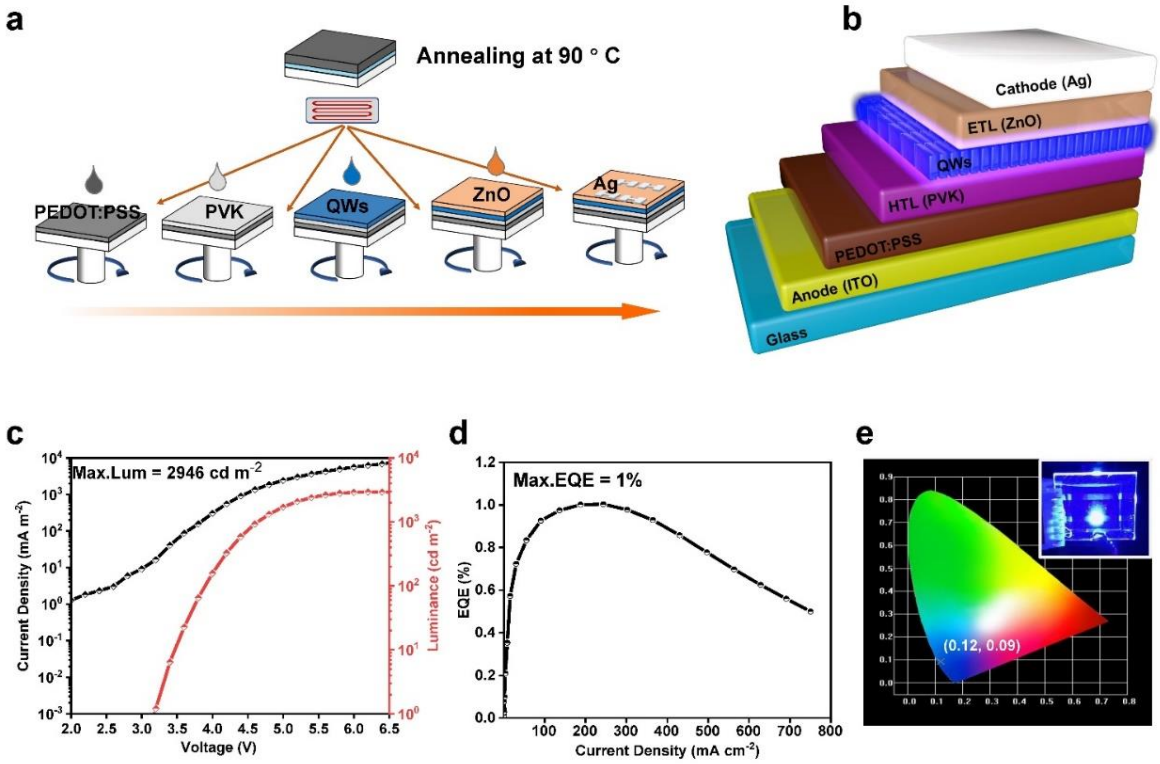

Figure 5. Performance of the LEDs based on the QWs. (a) Illustration of the all-solution process for preparing WD-synthesized QWs-based LEDs. (b) Device structure image. (c) J-V-L profiles; (d) EQE performance. (e) CIE index for the WD-synthesized QWs-based LEDs.

We have fabricated LEDs based on the WD-synthesized QWs via the all-solution process, illustrated in Figure 5a. This multilayered structure (Figure 5b) is comprised of indium tin oxide (ITO)-coated glass substrate / poly (3,4-ethylenedioxythiophene) polystyrenes sulfonate (PEDOT: PSS) / Polyvinyl carbazole (PVK) / $CsPbBr_3$ QWs / zinc oxide (ZnO) / Ag. The typical electrodes (cathode and anode) are equipped to achieve carriers (electrons and holes) injection. The injected electrons and holes drift into the QWs layer through electron-transport layer (ETL) and hole-transport layer (HTL), respectively, achieving radiative recombination to emit photons. The QWs are processed by ligand exchange to prepare LEDs according to our previous work. [3d] Further detail related to the QWs can be found in Figures S14-19, and Table S6. The current density-voltage-luminance (J-V-L) profiles of the device are shown in Figure 5c. The peak luminance of the LEDs is 2946 cd m^{-2}, which is the best performance for deep-blue LEDs based on perovskites QWs reported so far. The best-performing EQE (Figure 5d) of the LEDs is 1% at the current density of 188 mA cm^{-2}. Furthermore, the blue emission of the LEDs corresponds to the CIE (Commission Internationale de L'Eclairage) color coordinates of (0.12,0.09) (Figure 5e), satisfying both the National Television System Committee (NTSC) standard and the Rec. 2020 standards, thus indicating their excellent potential for display applications.

Conclusion

We have devised a water-driven synthesis strategy to obtain strong-confined $CsPbBr_3$ QWs of homogenized size and excellent crystallinity. Water in the reaction system controlled the orientation of the ligand distribution on the surface of the QWs, inducing better orientational crystallization of the QWs via an Ostwald ripening process that phagocytizes unstable nanocrystals. Consequently, the WD-synthesized QWs presented a deep-blue emission of 456 nm, narrow FWHM of 20 nm, and high PLQY of 94%, which is attributed to the great crystal quality, uniform size and morphology distribution. TA analysis verified the excellent optical performance of the WD-synthesized QWs, as a result of reduced surface defects and the suppressed non-radiative recombination dynamics. Based on the WD-synthesized QWs, we have fabricated blue LEDs via the all-solution process, gaining an EQE of 1% and outstanding luminance of 2946 cd m^{-2}, which is one of the highest luminance records for perovskites QW-based LEDs reported so far. Further studies are now required to further improve the operational efficiency and stability of QW-based LEDs, and explore further potential commercial applications of such QWs.

Acknowledgements

This work was supported by the Beijing Municipal Natural Science Foundation (2222061), Guangdong Basic and Applied Basic Research Foundation (2022A1515140007), National Natural Science Foundation of China (51961135107, 51774034). X.W. acknowledges the China Scholarship Council and the University of Leeds for a PhD scholarship.

Conflict of Interest

The authors declare no conflict of interest.

Keywords: Colloidal quantum wells; metal halide perovskite; deep-blue; water-driven synthesis; light-emitting diodes

References

[1] a) L. Protesescu, S. Yakunin, M. I. Bodnarchuk, F. Krieg, R. Caputo, C. H. Hendon, R. X. Yang, A. Walsh, M. V. Kovalenko, *Nano Lett.* **2015**, *15*, 3692-3696; b) F. Krieg, S. T. Ochsenbein, S. Yakunin, S. Ten Brinck, P. Aellen, A. Suess, B. Clerc, D. Guggisberg, O. Nazarenko, Y. Shynkarenko, S. Kumar, C. J. Shih, I. Infante, M. V. Kovalenko, *ACS Energy Lett.* **2018**, *3*, 641-646; c) J. Shamsi, A. S. Urban, M. Imran, L. De Trizio, L. Manna, *Chem. Rev.* **2019**, *119*, 3296-3348; d) H. He, S. Mei, Z. Wen, D. Yang, B. Yang, W. Zhang, F. Xie, G. Xing, R. Guo, *Small* **2022**, *18*, 2103527.

[2] a) M. Xie, J. Guo, X. Zhang, C. Bi, L. Zhang, Z. Chu, W. Zheng, J. You, J. Tian, *Nano Lett.* **2022,** *22*, 8266-8273; b) Y. K. Wang, K. Singh, J. Y. Li, Y. Dong, X. Q. Wang, J. M. Pina, Y. J. Yu, R. Sabatini, Y. Liu, D. Ma, J. Liu, Z. Liu, Y. Gao, O. Voznyy, W. Ma, M. K. Fung, L. S. Liao, E. H. Sargent, *Adv. Mater.* **2022**, *34*, 2200854; c) Y. Dong, Y. K. Wang, F. Yuan, A. Johnston, Y. Liu, D. Ma, M. J. Choi, B. Chen, M. Chekini, S. W. Baek, L. K. Sagar, J. Fan, Y. Hou, M. Wu, S. Lee, B. Sun, S. Hoogland, R. Quintero-Bermudez, H. Ebe, P. Todorovic, F. Dinic, P. Li, H. T. Kung, M. I. Saidaminov, E. Kumacheva, E. Spiecker, L. S. Liao, O. Voznyy, Z. H. Lu, E. H. Sargent, *Nat. Nanotechnol.* **2020**, *15*, 668-674.

[3] a) M. Zhang, C. Zuo, J. Tian, L. Ding, *Journal of Semiconductors* **2021**, *42*,

070201; b) G. Zou, Z. Chen, Z. Li, H.-L. Yip, *Acta Physico Chimica Sinica* **2021**, *37*, 2009002; c) Z. Yao, C. Bi, A. Liu, M. Zhang, J. Tian, *Nano Energy* **2022**, *95*, 106974.

[4] a) M. Xie, J. Tian, *J. Phys. Chem. Lett*. **2022**, *13*, 1962-1971; b) Z. Tan, J. Luo, L. Yang, X. Li, Z. Deng, L. Gao, H. Chen, J. Li, P. Du, G. Niu, J. Tang, *Advanced Optical Materials* **2019**, *8*, 1901094; c) G. Nedelcu, L. Protesescu, S. Yakunin, M. I. Bodnarchuk, M. J. Grotevent, M. V. Kovalenko, *Nano Lett.* **2015**, *15*, 5635-5640; d) J. Xing, Y. Zhao, M. Askerka, L. N. Quan, X. Gong, W. Zhao, J. Zhao, H. Tan, G. Long, L. Gao, Z. Yang, O. Voznyy, J. Tang, Z. H. Lu, Q. Xiong, E. H. Sargent, *Nat. Commun.* **2018**, *9*, 3541.

[5] a) C. Zhao, Z. He, P. Wangyang, J. Tan, C. Shi, A. Pan, L. He, Y. Liu, *ACS Applied Nano Materials* **2022**, *5*, 13737-13744; b) Y. Fu, S. Poddar, B. Ren, Y. Xie, Q. Zhang, D. Zhang, B. Cao, Y. Tang, Y. Ding, X. Qiu, L. Shu, J. F. Liao, D. B. Kuang, Z. Fan, *ACS Nano* **2022**, *16*, 8388-8398; c) A. Liu, C. Bi, J. Tian, *Advanced Functional Materials* **2022,** *32***,** 2207069; d) C. Bi, Z. Yao, X. Sun, X. Wei, J. Wang, J. Tian, *Adv. Mater.* **2021**, *33*, 2006722; e) Y. Wang, X. Liu, Q. He, G. Chen, D. Xu, X. Chen, W. Zhao, J. Bao, X. Xu, J. Liu, X. Wang, *Advanced Functional Materials* **2021**, *31*, 2011251; f) G. Raino, N. Yazdani, S. C. Boehme, M. Kober-Czerny, C. Zhu, F. Krieg, M. D. Rossell, R. Erni, V. Wood, I. Infante, M. V. Kovalenko, *Nat. Commun.* **2022**, *13*, 2587; g) J. Pan, X. Li, X. Gong, J. Yin, D. Zhou, L. Sinatra, R. Huang, J. Liu, J. Chen, I. Dursun, A. M. E. Zohry, M. I. Saidaminov, H. Sun, O. F. Mohammed, C. Ye, E. H. Sargent, O. M. Bakr, *Angew. Chem. Int. Ed.* **2019**, *58*, 16077-16081; h) C. Bi, Z. Yao, J. Hu, X. Wang, M. Zhang, S. Tian, A. Liu, Y. Lu, N. Leeuw, M. Sui, J. Tian, *ACS Energy Lett.* **2023**, *8*, 731–739; i) Y. J. Yoon, Y. Chang, S. Zhang, M. Zhang, S. Pan, Y. He, C. H. Lin, S. Yu, Y. Chen, Z. Wang, Y. Ding, J. Jung, N. Thadhani, V. V. Tsukruk, Z. Kang, Z. Lin, *Adv. Mater*. **2019**, *31*, 1901602.

[6] a) Q. Jan, S. Nabi, F. Ahmad Sofi, M. Ahmad Bhat, *Spectrochimica Acta Part A: Molecular and Biomolecular Spectroscopy* **2022**, *270*, 120749; b) M. Xie, Y. Zhu, R. Wang, J. Tian, *J. Phys. Chem. Lett.* **2021**, *12*, 10735-10741; c) M. Olutas, B. Guzelturk, Y. Kelestemur, A. Yeltik, S. Delikanli, H. V. Demir, *ACS Nano* **2015**, *9*, 5041-5050; d) Q. Li, T. Lian, *Chem Sci* **2018**, *9*, 728-734; e) B. Liu, Y. Altintas, L. Wang, S. Shendre, M. Sharma, H. Sun, E. Mutlugun, H. V. Demir, *Adv. Mater.* **2020**, *32*, 1905824; f) C. Zhou, H. Lin, Q. He, L. Xu, M. Worku, M. Chaaban, S. Lee, X. Shi, M.-H. Du, B. Ma, *Materials Science and Engineering: R: Reports* **2019**, *137*, 38-65.

[7] a) J. Cho, H. Jin, D. G. Sellers, D. F. Watson, D. H. Son, S. Banerjee, *Journal of Materials Chemistry C.* **2017**, *5*, 8810-8818; b) Z. Wen, Z. Cui, H. He, D. Yang, S. Mei, B. Yang, Z. Xiong, S. Song, R. Bao, W. Zhang, G. Xing, F. Xie, R. Guo, *Journal of Materials Chemistry C.* **2022**, *10*, 9834 - 9840.

[8] H. Wang, F. Ye, J. Sun, Z. Wang, C. Zhang, J. Qian, X. Zhang, W. C. H. Choy, X. W. Sun, K. Wang, W. Zhao, *ACS Energy Letters* **2022**, *7*, 1137-1145.

[9] a) D. Ma, K. Lin, Y. Dong, H. Choubisa, A. H. Proppe, D. Wu, Y. K. Wang, B. Chen, P. Li, J. Z. Fan, F. Yuan, A. Johnston, Y. Liu, Y. Kang, Z. H. Lu, Z. Wei, E. H. Sargent, *Nature* **2021**, *599*, 594-598; b) Y. K. Wang, D. Ma, F. Yuan, K. Singh, J. M. Pina, A. Johnston, Y. Dong, C. Zhou, B. Chen, B. Sun, H. Ebe, J. Fan, M. J. Sun, Y. Gao, Z. H. Lu, O. Voznyy, L. S. Liao, E. H. Sargent, *Nat. Commun.* **2020**, *11*, 3674.

[10] a) W. Wang, M. Zhang, Z. Pan, G. M. Biesold, S. Liang, H. Rao, Z. Lin, X. Zhong, *Chem. Rev.* **2022**, *122*, 4091-4162; b) S. Pan, Y. Chen, Z. Wang, Y.i Harn, J. Yu, A. Wang, M. J. Smith, Z. Li, V. V. Tsukruk, J. Peng, Z. Lin, *Nano Energy*, **2020**, *77*, 105043; c) Y. He, Y. J. Yoon, Y. W. Harn, G. V. Biresold-MxGee, S. Liang, C. H. Lin, V. V. Tsukruk, N. Thadhani, Z. Kang, Z. Lin, *Sci. Adv*. **2019**, *5*, eaax4424; d) S. Liang, S.

He, M. Zhang, Y. Yan, T. Jin, T. Lian, Z. Lin, *J. Am. Chem. Soc.* **2022**, *144*, 12901–12914.

[11] a) X. Zhang, X. Bai, H. Wu, X. Zhang, C. Sun, Y. Zhang, W. Zhang, W. Zheng, W. W. Yu, A. L. Rogach, *Angew. Chem. Int. Ed.* **2018**, *57*, 3337-3342; b) C. Otero-Martinez, J. Ye, J. Sung, I. Pastoriza-Santos, J. Perez-Juste, Z. Xia, A. Rao, R. L. Z. Hoye, L. Polavarapu, *Adv. Mater.* **2022**, *34*, 2107105.

[12] Z. Z. Ma, Z. F. Shi, L. T. Wang, F. Zhang, D. Wu, D. W. Yang, X. Chen, Y. Zhang, C. X. Shan, X. J. Li, *Nanoscale* **2020**, *12*, 3637-3645.

[13] M. Liu, Q. Wan, H. Wang, F. Carulli, X. Sun, L. Kong, Q. Zhang, C. Zhang, Q. Zhang, S. Brovelli, L. Li, *Nature Photonics* **2021**, *15*, 379-385.

[14] M. Ren, S. Cao, J. Zhao, B. Zou, R. Zeng, *Nanomicro Lett.* **2021**, *13*, 163.

[15] a) J. Pan, Y. Shang, J. Yin, M. De Bastiani, W. Peng, I. Dursun, L. Sinatra, A. M. El-Zohry, M. N. Hedhili, A. H. Emwas, O. F. Mohammed, Z. Ning, O. M. Bakr, *J. Am. Chem. Soc.* **2018**, *140*, 562-565; b) B. Akbali, G. Topcu, T. Guner, M. Ozcan, M. M. Demir, H. Sahin, *Physical Review Materials* **2018**, *2,* 034601; c) H. M. Ghaithan, Z. A. Alahmed, S. M. H. Qaid, A. S. Aldwayyan, *ACS Omega* **2021**, *6*, 30752-30761.

[16] a) Z. Li, E. Hofman, A. H. Davis, M. M. Maye, W. Zheng, *Chem. Mater.* **2018**, *30*, 3854-3860; b) Y. Liu, F. Li, Q. Liu, Z. Xia, *Chem. Mater.* **2018**, *30*, 6922-6929.

[17] a) Y. Yang, J. Wu, X. Wang, Q. Guo, X. Liu, W. Sun, Y. Wei, Y. Huang, Z. Lan, M. Huang, J. Lin, H. Chen, Z. Wei, *Adv. Mater.* **2020**, *32*, 1904347

[18] a) J. Chen, D. Jia, J. Qiu, R. Zhuang, Y. Hua, X. Zhang, *Nano Energy* **2022**, *96,* 107140; b) J. Shi, F. Li, Y. Jin, C. Liu, B. Cohen-Kleinstein, S. Yuan, Y. Li, Z. K. Wang, J. Yuan, W. Ma, *Angew. Chem. Int. Ed.* **2020**, *59*, 22230-22237.

[19] F. Liu, Y. Zhang, C. Ding, S. Kobayashi, T. Izuishi, N. Nakazawa, T. Toyoda, T. Ohta, S. Hayase, T. Minemoto, K. Yoshino, S. Dai, Q. Shen, *ACS Nano* **2017**, *11*, 10373-10383.

[20] a) N. Mondal, A. Samanta, *Nanoscale* **2017**, *9*, 1878-1885; b) H. Chung, S. I. Jung, H. J. Kim, W. Cha, E. Sim, D. Kim, W. K. Koh, J. Kim, *Angew. Chem. Int. Ed.* **2017**, *56*, 4160-4164; c) C. Villamil Franco, G. Trippe-Allard, B. Mahler, C. Cornaggia, J. S. Lauret, T. Gustavsson, E. Cassette, *J. Phys. Chem. Lett.* **2022**, *13*, 393-399.

[21] a) C. Luo, C. Yan, W. Li, F. Chun, M. Xie, Z. Zhu, Y. Gao, B. Guo, W. Yang, *Advanced Functional Materials* **2020**, *30*, 2000026; b) C. Bi, J. Hu, Z. Yao, Y. Lu, D. Binks, M. Sui, J. Tian, *Advanced Functional Materials* **2020**, *30*, 2005990; c) N. S. Makarov, S. Guo, O. Isaienko, W. Liu, I. Robel, V. I. Klimov, *Nano Letters* **2016**, *16*, 2349-2362.

[22] B. R. Sutherland, E. H. Sargent, *Nature Photonics* **2016**, *10*, 295-302.

[23] a) J. Chen, D. Liu, M. J. Al-Marri, L. Nuuttila, H. Lehtivuori, K. Zheng, *Science China Materials* **2016**, *59*, 719 - 727. b) Y. He, Y. Liang, S. Liang, Y. W. Harn, Z. Li, M. Zhang, D. Shen, Z. Li, Y. Yan, X. Pang, Z. Lin, *Angew. Chem. Int. Ed.* **2021**, *60*, 7259-7266.

Table of Contents

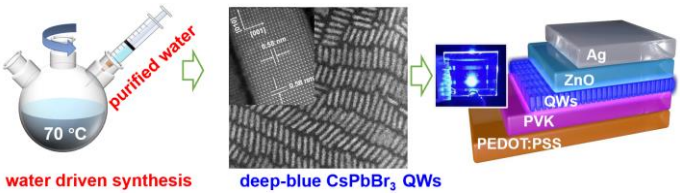

A creatively water-driven strategy is devised to obtain size-homogenized and strongly confined deep-blue perovskite quantum wells (QWs) with remarkable stability and high photoluminescence quantum yield of 94%. The electroluminescent devices based on the QWs show high luminance of 2946 cd m^{-2}, demonstrating state-of-the-art brightness for perovskite QWs based devices.